https://doi.org/10.15407/ufm.25.04.787

V.V. GIRZHON [1,*], O.V. SMOLYAKOV [1,], V.L. GRESHTA [1,***], V.V. YEMELIANCHENKO [1,****], and A.Sh. RAZZOKOV [2]**

[1] National University 'Zaporizhzhia Polytechnic',
64 Zhukovsky Str., UA-69063 Zaporizhzhia, Ukraine
[2] Urgench State University,
14 Khamid Alimzhan Str., UZ-220100 Urgench City, Uzbekistan

* vgirzhon@gmail.com, ** asmolyakov972@gmail.com,
*** greshtaviktor@gmail.com, **** emelyanchenkovlad@gmail.com

LASER TREATMENT OF TITANIUM ALLOYS

The structural and phase states of surface layers of the titanium VT1-0, VT3-1, VT-6 and VT-8 alloys after laser treatment in various gas environments, VT25-U alloy after twist extrusion and subsequent laser treatment, and VT1-0 alloy after laser alloying with powders of pure elements Fe, Co, Ni are investigated *via* the x-ray and metallographic analysis methods. As shown, the mentioned types of treatments lead to an increase in the surface-layers' microhardness values. The influence of the surrounding gas atmosphere and the titanium-alloy chemical composition on the structure-formation processes during their laser melting and on the microhardness value of the treated layers is analysed. The effect of laser treatment of the surface of sintered single-phase powder titanium VT1-0-type alloys on the porosity level in the melting zone is investigated. As established, the microhardness in the laser-melting zone of the VT25U alloy exceeds the samples' microhardness after heat treatments and twist extrusion. Therefore, the presented laser surface-treatment modes act as an effective method of titanium-alloy surface treatment, since they have a qualitative effect on structure that, in turn, leads to an improvement in the mechanical characteristics of the surface layers.

Keywords: laser treatment, laser alloying, melting zone, martensitic transformation, microhardness, phase composition.

Citation: V.V. Girzhon, O.V. Smolyakov, V.L. Greshta, V.V. Yemelianchenko, and A.Sh. Razzokov, Laser Treatment of Titanium Alloys, *Progress in Physics of Metals*, **25**, No. 4: 787–821 (2024)

1. Introduction

The successful development of modern science-intensive technologies involves the use of materials with high physical and mechanical properties. Such materials include titanium and alloys based on it. The wide use range of titanium alloys is due to the complex properties inherent in this class of materials: high specific strength, rather low density, corrosion resistance in many aggressive environments [1–3]. The production of a whole range of machine parts and structural elements for responsible purposes is impossible without the use of Ti-alloys. Their most widespread application is in aircraft and shipbuilding, cosmonautics, medicine, chemical engineering, the production of sports equipment, *etc.* [4–6].

Having a complex of unique properties, titanium alloys are also characterized by several disadvantages that limit their use as structural materials. These include, for example, the high cost of alloys and gas saturation during high-temperature operations. However, the most serious disadvantages of titanium alloys are low tribotechnical properties, which are caused by the low hardness and titanium's tendency to seize during working in friction pairs. Another feature of titanium is its high chemical activity. Therefore, during exposure to air, titanium oxidizes at a high rate with the formation of a thin, dense film, which subsequently ensures its corrosion resistance. However, if the film is destroyed in the interaction process with another body, the material coefficient of friction increases sharply, which leads to surface layer burrs and accelerated product wear [7].

Thus, their surface strengthening is an urgent task today. Solving this problem will lead to a sharp expansion of titanium alloys' scope of use.

Conventionally, all strengthening methods can be divided into two large groups: volume and surface. Volume hardening methods include alloying, heat treatment, rolling, plastic deformation, *etc.* [8–11]. With such strengthening, the entire material volume acquires approximately the same structural changes. It should be noted that alloying and heat treatment cannot significantly increase titanium-alloys' antifriction properties.

In many cases, product surface strengthening is more rational: surface alloying, surface hardening or wear-resistant materials surfacing, protective coatings application, *etc.* The reason for this is that during the mechanisms' operation, the main load falls on the parts' surface layers that are in contact with each other. In the case of implementing these methods, only thin surface layers are strengthened, while the inner material volume is not significantly strengthened and remains in a viscous state, which can have a favourable effect on the products' reliability. This approach to solving the strengthening problem allows us to save on expensive alloying components.

Today, many specific methods of titanium alloy surface strengthening are proposed. The choice of the optimal strengthening technology is based

on the requirements for the final product during its operation. Titanium, being in a hot state, tends to be saturated with the interstitial elements: oxygen, nitrogen, and hydrogen. Therefore, nitriding, oxygen saturation, and cementation are used to strengthen titanium alloys. One of the main industrial methods of titanium alloys' surface strengthening is thermodiffusion saturation of the surface layers with nitrogen (nitriding) [12–18]. Traditional methods of such treatment are usually carried out at temperatures of 1123–1223 K that causes an increase in the grain size, hydrogen diffusion and, as a result, a deterioration of the product's mechanical properties. The main disadvantages of this treatment are low productivity, high-energy consumption, and insufficient reinforced layer depth. For obtaining strengthened layers of great thickness, long-term treatment at elevated temperatures is carried out. The result is a material-structure coarsening (grain growth) and, as a consequence, a decrease in the alloy mechanical characteristics [19]. Materials strengthened in this way are not recommended to be used for the manufacture of responsible-purpose parts.

In addition to chemical and thermal treatment, the application of protective coatings by sputtering and deposition methods is used to increase the titanium alloy surface strengthening. The disadvantages of characteristics of these technologies are the small coatings thickness and the low level of their adhesive properties [20–22].

Recently, titanium alloys surface strengthening methods based on the use of concentrated energy sources (high-frequency currents, electron and laser beams) have become widespread. The main advantages of these strengthening methods are high rates of material heating and cooling in the treatment process and high process productivity. At the same time, electron-beam and laser-treatment (LT) technologies turned out to be the most common.

The technology of materials treatment with electron beams has been studied in detail [23–26]. It can be used both for workpieces surface heat treatment or protective-coatings' surfacing and for welding structures. The electron-beam technological capabilities are close to those of a laser, but electron-beam treatment is carried out in a vacuum. This treatment is characterized by a high thermal efficiency (up to 0.75), and it allows for minimisation of the number of pores and cracks formed. One of the main problems that arise during the powerful electron-beam installation operation is the need to protect personnel from x-ray radiation.

Laser alloying is one of the promising methods for improving the mechanical properties of the titanium-alloys' surface layers [27–32]. This perspective exists due to the following factors: significant energy savings, high process productivity and minimal parts deformation [33]. Compared to traditional methods, surface modification by using a laser has several advantages for ensuring the performance of friction-pairs' surfaces: the possibility of local treatment of a certain given area, rapid heating and

cooling of the treatment zone subject, the formation of strong dispersed intermetallic phases in the laser action zone, *etc.* [34, 35]. The surfaces' laser-alloying technology ensures the production of coatings characterized by a different degree of alloying materials dissolution by the base metal. The resulting coating is characterized by a high level of adhesive properties since the matrix material directly participates in the structure formation process. The coating quality and thickness largely depend on the laser treatment parameters, the alloying mixture composition and fraction, as well as on the matrix material composition and properties [36].

Despite the significant scientific-publications' number in the field of titanium-alloys' laser treatment, the number of studies on the structure-formation processes during such treatment is still insufficient; in particular, few studies are devoted to treatment using pulsed lasers. However, the use of a pulsed, for example, YAG laser allows surface treatment with high (about 10^4 K/s) heating and cooling rates [37]. As a result, depending on the laser radiation technological parameters and the gas atmosphere, in which the treatment took place, significant structural changes can be expected in the laser action zone: an increase in the dispersion degree of the structure, a volume ratios redistribution of the α- and β-phases, the formation of supersaturated solid solutions, dispersed oxides or nitrides, a change in the type of $\beta \rightarrow \alpha$ phase transition, *etc.* [38].

Based on the above, the purpose of this work is to study the structure formation processes in the titanium-alloys' surface layers during various types of pulsed laser treatments of their surface.

2. Materials and Methods

Samples of industrial titanium alloys were selected for research, the dimensions of which were not smaller than $10 \times 10 \times 3$ mm^3 (Table 1).

Laser treatment of the samples' flat surfaces was performed on a pulsed YAG laser (λ = 1.06 μm) at different radiation power densities, pulse durations, and pulse repetition frequencies in different atmospheres (argon, nitrogen, air). Laser alloying was carried out in a protective argon environment using the coating method (binder is BF-6 glue) with 30%

Table 1. **Chemical composition of titanium alloys**

Alloy	Chemical composition, mas.%														
	Ti	Al	V	Zr	Mo	Cr	W	Sn	Si	Fe	O	H	N	C	Others
VT1-0	basis	—	—	—	—	—	—	—	0.1	0.15	0.20	0.010	0.04	0.07	0.3
VT3-1	basis	5.8	—	0.5	2.8	1.3	—	—	0.3	0.40	0.15	0.015	0.05	0.10	0.3
VT-6	basis	6.1	4.0	0.3	—	—	—	—	0.1	0.60	0.20	0.015	0.05	0.10	0.3
VT-8	basis	6.3	—	0.5	3.1	—	—	—	0.2	0.30	0.15	0.015	0.05	0.10	0.3
VT25-U	basis	6.6	—	3.7	3.9	—	1.1	1.4	0.3	0.15	0.15	0.01	0.04	0.10	0.3

laser spots overlapping. Pure elements powders of Fe, Co, and Ni with a fraction size not exceeding 50 μm were chosen as alloying components. The coating thickness was 150 μm. The alloyed layer depth was 150–200 μm.

The phase composition of the samples' surface layers after various types of laser treatments was controlled by the x-ray diffraction (XRD) method (RIGAKU MULTIFLEX, filtered CuK_α radiation), the structural components sizes were determined metallographically (EPIQUANT), the microhardness distribution by the laser action zone depth and on the surface was determined using a PMT-3.

3. Results and Discussion

3.1. Laser Melting in Different Gas Atmospheres

LT is a high-tech type of thermal impact on the metal-alloys' surface layers to improve their physical and mechanical properties. Usually, such treatment is carried out in an air atmosphere. However, depending on the chemical activity of the material to be processed, the influence of the surrounding atmosphere can have a significant impact both on the structure formation processes in the laser action zone (LAZ) and on the treated surface properties. Since titanium is a chemically active metal, at the first stages, the influence of the surrounding atmosphere on the structure and some mechanical properties of the surface layers after LT were investigated in different gas atmospheres (argon, air, nitrogen).

Industrial titanium alloys VT1-0, VT3-1, VT-6, and VT-8 were chosen as materials for research (Table 1).

3.1.1. VT1-0 Alloy

At the first stage, as a model material, technically pure titanium VT1-0 was chosen for research. LT in surface melting mode was carried out with power density q = 1.2 GW/m^2, pulse duration τ = 2.00 ms, and pulse repetition frequency ν = 3 Hz.

In the initial state, the samples were single-phase: only reflections from the α-phase of titanium were detected (Fig. 1, *a*). After LT in an argon atmosphere, the phase composition did not change (Fig. 1, *b*). The sample treatment in the air atmosphere led to significant changes in the LAZ phase composition. Three phases were observed: α-Ti, tetragonal oxide TiO_2 and cubic nitride TiN (Fig. 1, *c*). Laser melting of the samples in a nitrogen flow made it possible to record reflections from two lattices: α-Ti and TiN nitride (Fig. 1, *d*) [39].

The oxides and nitrides formation of a significant amount in LAZ is easily explained by the enrichment of the melt with oxygen and nitrogen and the high titanium chemical activity at high temperatures. A rather noticeable increase in the α-titanium lattice parameters after laser melting

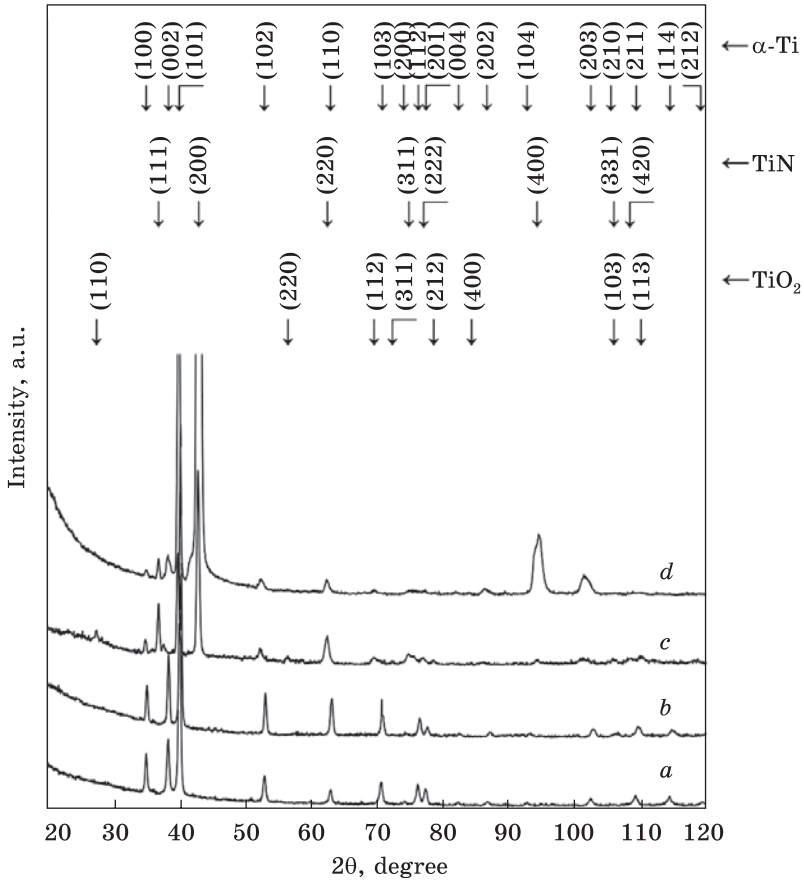

Fig. 1. XRD-patterns from the surface layers of VT1-0 alloy samples in the initial state (*a*) and after LT in Ar (*b*), air (*c*), and N (*d*) atmospheres [39]

Table 2. **Lattice parameters of the α-Ti after surface LT in a nitrogen atmosphere [39]**

Initial state	LT in a nitrogen atmosphere
Lattice parameters, nm	
$a = 0.29549 \pm 0.00024$ $c = 0.46880 \pm 0.00024$	$a = 0.29732 \pm 0.00003$ $c = 0.47055 \pm 0.00009$

Table 3. **Phase composition and microhardness of the VT1-0 alloy surface layers after laser treatment [39]**

Treatment type	Phase composition	Microhardness H_μ, GPa
Initial state	α-Ti	1.8 ± 0.01
LT in an argon atmosphere	α-Ti	2.5 ± 0.01
LT in the air atmosphere	α-Ti, TiN, TiO_2	5.5 ± 0.02
LT in a nitrogen atmosphere	α-Ti, TiN	8.1 ± 0.03

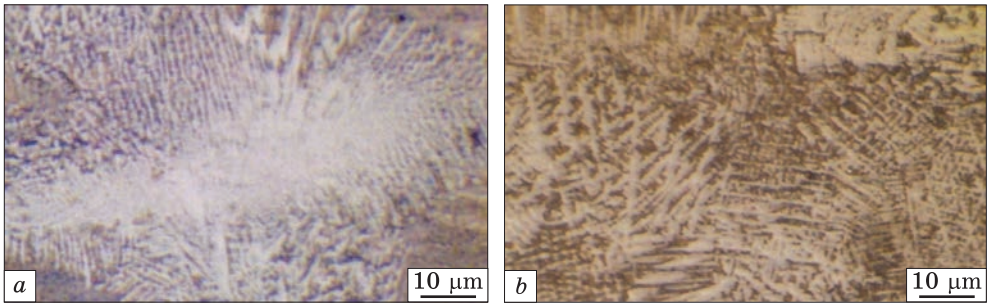

Fig. 2. The microstructure of the samples after LT in air (*a*) and nitrogen (*b*) atmospheres [39]

in a nitrogen atmosphere (Table 2) indicated that not all nitrogen atoms took part in the formation of the nitride; some of them could enter the interstitial sites of the h.c.p. lattice, forming a solid solution of nitrogen in the α-Ti lattice. This follows directly from the analysis of Ti–O and Ti–N systems state diagrams [40, 41]: at high temperatures, the solubility of oxygen and nitrogen in the α-titanium lattice increases several times. Moreover, since the melt-cooling rate was of about 10^4 K/s, a supersaturated solid solution of nitrogen in the titanium lattice at room temperature was formed, which led to an increase in lattice parameters.

It should be noted that, after LT in all atmospheres, a fairly significant redistribution of the maximum intensities on XRD-patterns showed, compared to the table values, which was probably caused by the crystalline texture presence that arose as a result of directed heat removal during melt rapid cooling.

Structural changes in the surface layers of the treated samples led to a change in their microhardness (Table 3), and an increase in microhardness was observed after all LTs.

It is significant that after LT in an argon atmosphere, the phase composition of the melted zone did not change. The grain size, as a result of melt high cooling rates, diminished significantly and amounted to 2–3 μm (at the initial state of 10–15 μm), which became the main reason for the increase in the microhardness value.

After treatment in air and nitrogen atmospheres, the increase in H_μ values, in addition to the increase in the dispersion degree of the structure (Fig. 2), was also influenced by the formation of small nitrides and supersaturated solid solutions of nitrogen and oxygen in the α-titanium lattice, *i.e.*, solid-solution strengthening.

3.1.2. VT3-1 Alloy

The VT3-1 alloy is a two-phase heat-resistant deformable alloy with fairly high strength. It is used for the production of forged and stamped parts that can be operated for a long time at temperatures of 673–723 K.

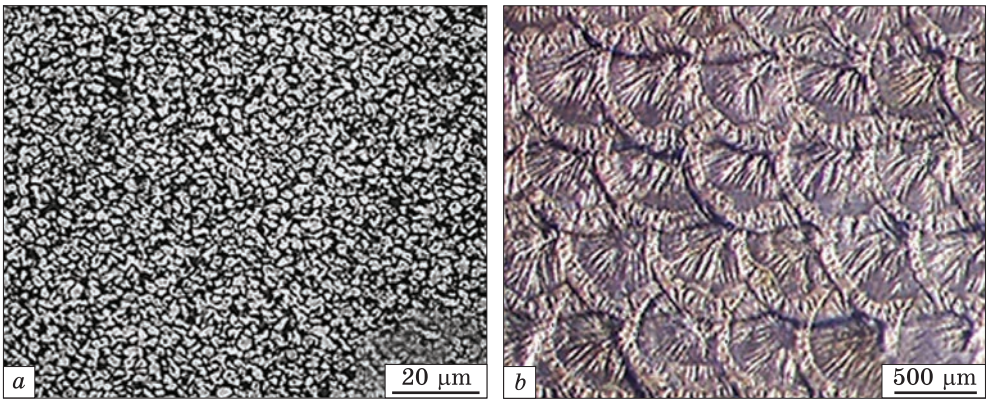

Fig. 3. Initial structure (*a*) and surface of VT3-1 alloy samples after laser melting in a nitrogen environment (*b*) [42]

According to the metallographic analysis data, in the initial state, α-Ti and β-Ti phases were observed in the alloy structure (Fig. 3, *a*). At the same time, the volume fraction of α-Ti did not exceed 65%. The alloy surface after laser melting is shown in Fig. 3, *b*.

Two phases were also detected in the original alloy structure (Fig. 4, *a*): h.c.p. solid solution based on α-Ti with lattice parameters $a = 0.2950 \pm \pm 0.0008$ nm and $c = 0.4683 \pm 0.0006$ nm and b.c.c. solid solution based on β-Ti with lattice parameter $a = 0.3306 \pm 0.0005$ nm.

After LT in an argon atmosphere, some expansion of the diffraction maxima from the α-phase lattice was observed (Fig. 4, *b*), which can be caused both by an increase in the phase dispersion degree and by the occurrence of internal stresses in the lattice. Reflections from the β-phase lattice were not observed, *i.e.*, the alloy turned out to be single-phase. This can be explained by the fact that, due to melting rapid cooling, the $\beta \rightarrow \alpha$-transformation occurred completely. At the same time, such a transformation occurs mainly by the martensitic $\beta \rightarrow \alpha'$ mechanism, which is not contradicted [43].

The change in parameters of the α-Ti lattice after LT in an argon environment (Table 4) occurred due to the formation of a supersaturated substitution solid solution of aluminium, molybdenum, and chromium, as the amount of alloying elements in the VT3-1 alloy exceeded their solubility in the α-Ti lattice at room temperature, and their atomic radii values were smaller compared to the titanium atomic radius [44].

The cross-section analysis of the LAZ made it possible to conditionally divide it into two areas (Fig. 5, *a*): the melting zone (MZ) with a needle-like structure (Fig. 5, *b*) and the two-phase thermal influenced zone (TIZ) depleted by β-Ti (Fig. 3, *c*). The depth values of the zones were approximately equal to 150–200 microns and 80–90 microns, respectively.

The average microhardness values in the melting zone obtained in an argon environment were slightly lower than in the initial state (H_μ =

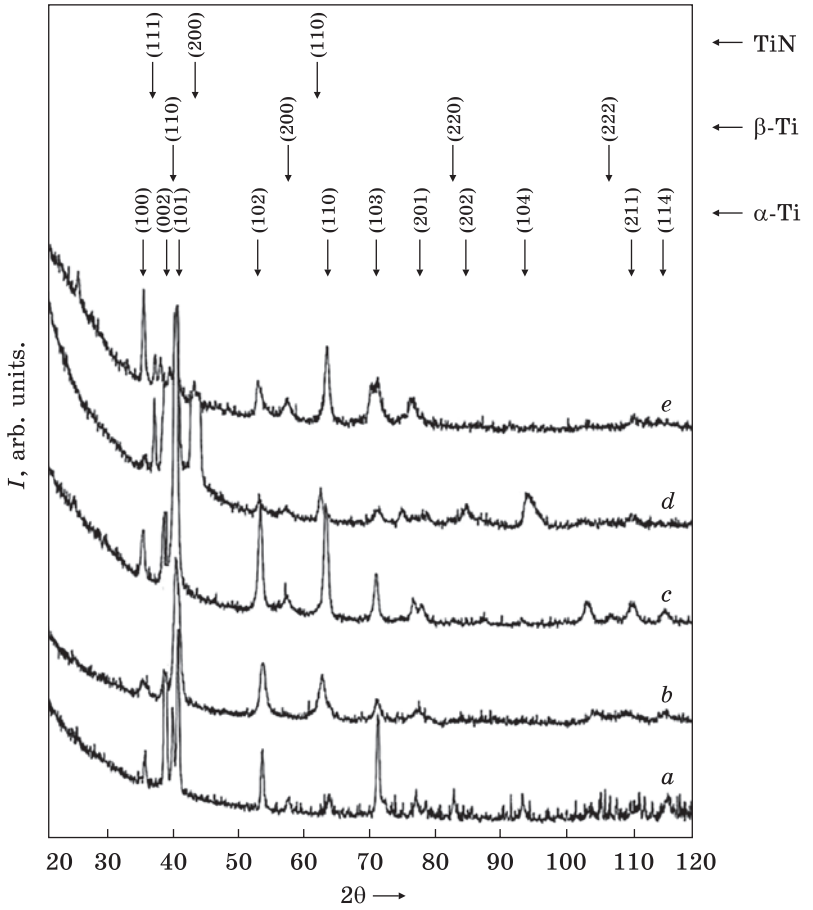

Fig. 4. XRD patterns from the VT3-1 Ti alloy surface samples: *a* — initial state; after laser melting: *b* — in Ar atmosphere; *c* — in Ar atmosphere with subsequent annealing in air; *d* — in N_2 atmosphere; *e* — in the air [42]

Table 4. **Lattice parameters of the α-Ti and the phase composition of the laser exposure zone after various types of treatment [42]**

Treatment type	Phase composition	Lattice parameters, nm
Initial state	α-Ti + β-Ti	$a = 0.2951 \pm 0.0008$ $c = 0.4682 \pm 0.0002$
Laser melting in an argon atmosphere ($q = 1.0$ GW/m^2)	α-Ti + α′-Ti	$a = 0.2948 \pm 0.0008$ $c = 0.4680 \pm 0.0011$
Laser melting in Ar atmosphere ($q = 1.0$ GW/m^2) + annealing in air atmosphere (773 K, 180 min)	α-Ti + β-Ti	$a = 0.2944 \pm 0.0008$ $c = 0.4669 \pm 0.0019$
Laser melting in a nitrogen atmosphere ($q = 1.0$ GW/m^2)	α-Ti + β-Ti + TiN	$a = 0.2929 \pm 0.0008$ $c = 0.4676 \pm 0.0012$
LT in pre-melting mode ($q = 0.5$ GW/m^2)	α-Ti + β-Ti + TiN	$a = 0.2933 \pm 0.0008$ $c = 0.4714 \pm 0.0019$

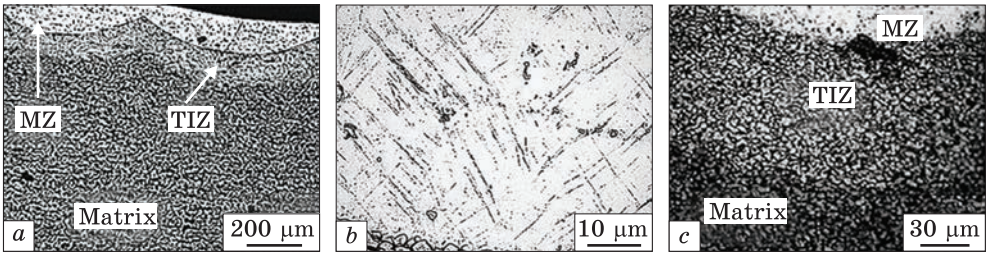

Fig. 5. Sample cross-section after laser melting in Ar environment (*a*); microstructure of the melting zone (*b*) and the thermally affected zone (*c*)

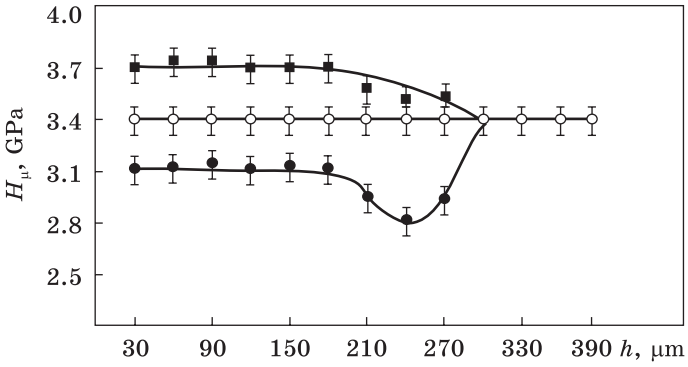

Fig. 6. Microhardness distribution of VT3-1 alloy along the TAZ depth for initial state (○), after laser melting in Ar environment (●), and in Ar environment with subsequent annealing in air (■)

= 3.3–3.4 GPa) and were approximately equal to 3.1–3.2 GPa (Fig. 6). This could be caused by the martensitic type of β→α′-transformation, which led to the absence of the β-Ti phase and, as a result, to a decrease in the microhardness values, which is consistent with [45]. It should be noted that, after laser melting, an increase in the dispersity degree of the α-phase (1–2 μm) was observed. This should lead to a significant increase in microhardness, but in this case, the decrease caused by the completeness of the β→α transformation turned out to be decisive.

The microhardness change by the depth of the LAZ ($H_\mu(h)$) turned out to be non-monotonic (Fig. 6). Microhardness values decreased to a depth of 210 μm (2.8–2.9 GPa). However, in the lower regions of the TIZ, the H_μ values increased almost to their values in the matrix. This character of the $H_\mu(h)$ dependence can be explained by some decrease in the amount of the β-phase in the TIZ upper part.

To remove internal stresses and disintegrate the metastable α′-phase, the samples melted in an argon environment were annealed in an air atmosphere at 773 K for 180 minutes. After this treatment, the two-phase structure (α-Ti + δ-Ti) was again observed by the XRD method (Fig. 4, *c*). At the same time, the microhardness values in LAZ increased slightly and amounted to 3.7–3.8 GPa in MZ and 3.5–3.6 GPa in TIZ. The increase in H_μ values can be associated both with a disintegration of the α′-phase with

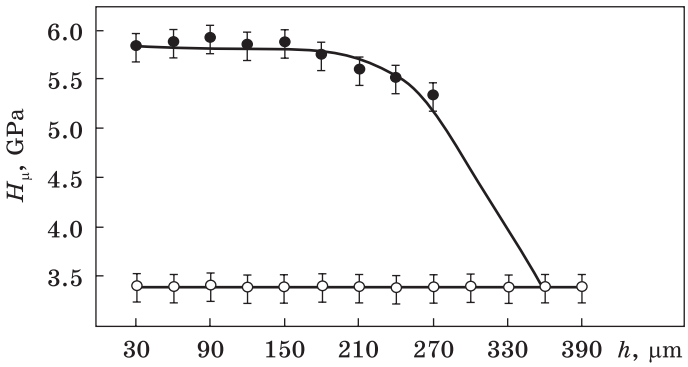

Fig. 7. Microhardness distribution by LAZ depth of VT3-1 alloy: ○ — initial state; ● — after laser melting in the nitrogen environment

the formation of a two-phase (α-Ti + δ-Ti) structure and with an increase in the dispersion degree of the structure as a result of laser treatment.

It can be assumed that, during laser melting in a nitrogen environment, a certain proportion of nitrogen atoms could not only be spent on the nitride formation, but also occupy octahedral interstitial sites in the hexagonal lattice of α-titanium, which would lead to the formation of an interstitial solid solution and, as a result, to an increase in the lattice parameters. Precise measurement of the α-Ti lattice parameters indeed revealed their increase (Table 4) that just confirms the validity of the proposed assumption.

The microhardness value in the surface layers increased significantly after such treatment (5.8–6.0 GPa in MZ and 5.3–5.5 GPa in TIZ) (Fig. 7). The increase in H_μ values after LT in a nitrogen environment can be caused several factors: an increase in the dispersion degree of the structure (as in the case of laser treatment in an argon environment), the formation of high-strength dispersed particles of titanium nitride TiN and the formation of a supersaturated interstitial solid solution of nitrogen in α-titanium.

It was shown above that laser melting of the surface (especially in a nitrogen environment) led to a significant increase in LAZ microhardness. However, this treatment also had a drawback: an increase in the surface roughness of the samples. This means that its final mechanical treatment is necessary for the product's operation. Therefore, studies of the surface layer structure after laser treatment with different beam power densities were conducted in the future to minimize the specified drawback.

It was established that a decrease in the radiation power density leads to a decrease in the surface roughness, but the depth of the LAZ also decreases. By XRD and metallographic methods, it was established that after the LT in nitrogen environment with a power density of $q \approx 950$ MW/m^2, there were no significant changes in the surface layer's structure, and the roughness slightly decreased (4–6 μm compared to 7–9 μm). Therefore, to avoid completely the surface melting, the laser power density was reduced to 500 MW/m^2.

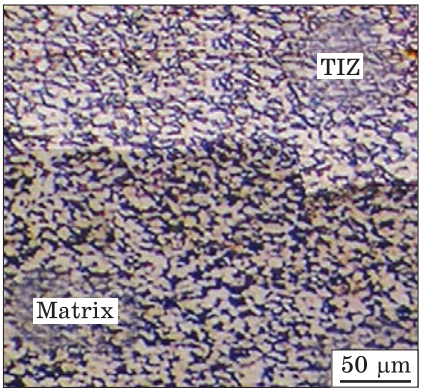

Fig. 8. The structure of the VT3-1 titanium alloy sample after laser treatment in a nitrogen environment with a power density of 500 MW/m^2 [42]

As a result of such treatment, MZ was no longer observed. Metallographic analysis showed the presence of only TIZ with a depth of about 90–120 microns in the sample cross-section (Fig. 8).

The phase composition of TIZ after LT in the air atmosphere (Fig. 4, *e*) contained three phases: α-Ti, β-Ti and a small amount of cubic titanium nitride. Despite the high chemical activity of titanium, titanium oxides were not detected [42]. A slight increase in the parameters of the α-Ti lattice may indicate the formation of a solid solution of nitrogen (oxygen) atoms in the h.c.p. titanium lattice, which could be the reason for the slight broadening of the diffraction maxima from the α-Ti lattice.

The microhardness values in the surface layers increased and were approximately equal to 4.4–4.5 GPa, which is associated with the formation of high-strength TiN nitride and the formation of a solid solution of nitrogen (oxygen) in the α-Ti lattice (solid solution hardening).

3.1.3. VT-6 Alloy

This is a high-strength, heat-resistant structural deformable two-phase (α+β) alloy; it is used for the manufacture of large-sized welded and assembled aircraft constructions, for the manufacture of gas cylinders that operate under internal pressure, and several other constructive elements, it is an analogue of the Grade5 (USA) alloy. Aluminium in Al–Ti–V alloys increases strength and heat-resistant properties, and vanadium contributes to increased plasticity. The alloy deforms well in a hot state and can be welded by all traditional methods, including diffusion welding [45–47].

LT of the alloy surface was performed with the following beam parameters: q = 1.2 GW/m^2, τ = 2.00 ms, ν = 3 Hz.

According to the data of the XRD analysis, the alloy structure in the initial state was two-phase: reflections from lattices of α- and β-solid solutions were recorded (Fig. 9, *a*). After LT in an argon atmosphere, only one α-phase was observed according to XRD data (Fig. 9, *b*). As a result of LT in air and nitrogen atmospheres, the XRD patterns showed reflections from lattices of three phases: α- and β-solid solutions and TiN nitride (Fig. 9, *c, d*).

The absence of the β-phase in the molten zone after treatment in an argon atmosphere can be explained by the fact that, as a result of the high cooling rates of the melt, the β→α-transformation could occur by means

of the martensitic mechanism, and it could be fully realized. The α′-phase formed as a result of this transformation, which is a solid solution of alloying elements in α-titanium, has a hexagonal lattice and a needle-like structure characteristic of martensite. It is known [44] that the implementation of the martensitic transformation in titanium alloys can lead to their weakening due to the completeness of the β→α-transformation and the absence of the β-phase. In our case, LT in an argon atmosphere led to some decrease in the microhardness values, despite a rather significant dispersion of the structure in LT (Table 5).

In the case of LT in air and nitrogen atmospheres, the martensitic transformation did not occur completely (weak reflections from the β-phase lattice were observed on the XRD patterns). The reason for the incomplete β→α-transformation may be the increased nitrogen solubility in the b.c.c. lattice of β-Ti, which could lead to an increase in the temperature of the β→α-transition [27, 43].

Precise measurements of the α-phase lattice parameters after LT in an argon atmosphere showed their decrease compared to the initial ones. This can be explained by the fact that as a result of the martensitic β→α transformation, a supersaturated substitution solid solution of vanadium and aluminium in the α-Ti lattice is formed. Since the atomic radii of vanadium and aluminium are smaller than the atomic radius of titanium, the α-phase lattice parameters turned out to be slightly lower than its parameters in the initial state (Table 6).

Table 5. **Phase composition and surface layers microhardness of the VT-6 alloy after LT in different gas atmospheres [39]**

Treatment type	Phase composition	Microhardness H_μ, GPa
Initial state	α-Ti, β-Ti	3.62 ± 0.01
LT in Ar atmosphere	α-Ti	3.50 ± 0.01
LT in the air atmosphere	α-Ti, β-Ti, TiN	4.74 ± 0.02
LT in N_2 atmosphere	α-Ti, β-Ti, TiN	5.31 ± 0.02

Table 6. **Lattice parameters of the α-phase after laser surface treatment in different atmospheres [39]**

Initial state	LT in the argon atmosphere	LT in the air atmosphere	LT in the nitrogen atmosphere
Lattice parameters, nm			
a = 0.29395 ± ± 0.00008	a = 0.29382 ± ± 0.00008	a = 0.29428 ± ± 0.00008	a = 0.29317 ± ± 0.00008
c = 0.46866 ± ± 0.00019	c = 0.46341 ± ± 0.00019	c = 0.46833 ± ± 0.00019	c = 0.46709 ± ± 0.00019

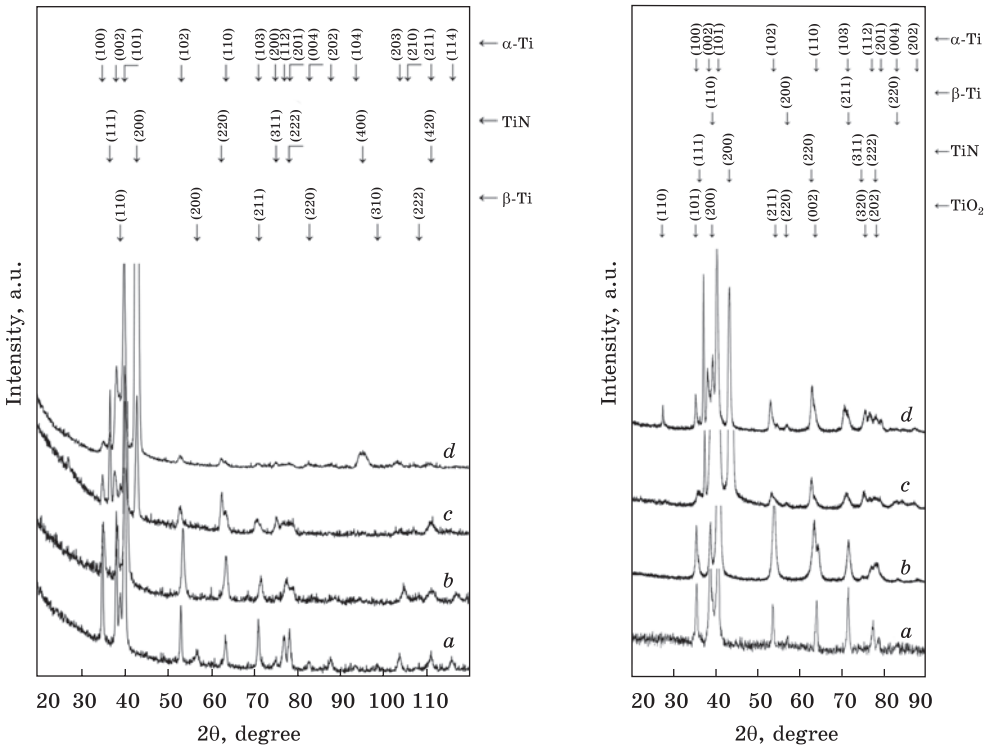

Fig. 9. XRD patterns from the surface layers of VT-6 alloy samples in their initial state (*a*) and after laser remelting in argon (*b*), air (*c*), and nitrogen (*d*) atmospheres [39]

Fig. 10. The same as in the previous figure, but for VT-8 alloy samples in the initial state (*a*) and after laser remelting in argon (*b*), nitrogen (*c*), and air (*d*) atmospheres [51]

According to the data presented in Table 6, LT in a nitrogen atmosphere also led to a slight decrease in the α-phase lattice parameters. It can be assumed that such parameter changes were caused by the complex influence of two factors. On the one hand, the formation of a supersaturated solid solution of vanadium and aluminium in the α-Ti lattice leads to a decrease in lattice parameters. On the other hand, in addition to the martensitic β→α transformation, there was also the formation of a supersaturated solid solution of nitrogen in the α-Ti lattice, which should have led to an increase in the lattice parameters. However, the influence of the first factor was more significant.

After LT in the air atmosphere, a slight increase in α-Ti lattice parameters was observed. In addition to the reasons listed above, the change in lattice parameters in this case may also have been influenced by the incorporation of oxygen atoms into the h.c.p. lattice with the formation of a supersaturated interstitial solid solution of oxygen in the α-Ti lattice, since the solubility of oxygen in titanium exceeds the solubility of nitrogen [44].

The results of microhardness measuring of the samples surface in the initial state and after LT in different atmospheres (Table 5) showed that treatment in an argon atmosphere (as in the case of the VT1-0 alloy) led to a slight decrease in microhardness associated with the complex action of two factors: H_μ values decreasing as a result of the martensitic transformation and an increase in the dispersion degree of the structure (increase in H_μ values).

The microhardness increase in LAZ after LT in an atmosphere of air and nitrogen is caused by the fact that, during such treatments, one more factor was added that caused an increase in microhardness, namely, the formation of a supersaturated interstitial solid solution of oxygen and nitrogen in α-titanium.

Thus, depending on the atmosphere, in which the laser treatment is performed and the selected modes of laser radiation, the change in microhardness in the laser treatment zone can be influenced by several factors: the completeness of the $\beta \rightarrow \alpha$ transformation, an increase in the dispersion degree of the structure, solid-solution strengthening due to the interstitial nitrogen and oxygen atoms in the h.c.p. titanium lattice and the formation of dispersed cubic titanium nitride.

3.1.4. VT-8 Alloy

The alloy belongs to heat-resistant structural deformable two-phase alloys and has a wide scope of use: it is used for obtaining ingots and manufacturing semi-finished products (sheets, strips, plates, rods, pipes, *etc.*) by deformation method; various parts of mechanisms that are operated at temperatures not higher than 750 K; parts of gas turbine blades of aircraft engines. The alloy is corrosion-resistant and provides higher strength and heat-resistant properties compared to the VT-6 alloy due to the high content of aluminium and silicon alloying, it can be thermally strengthened and deforms satisfactorily in the hot state [48–50].

Laser treatment was performed in argon, air and nitrogen atmospheres with a radiation power density q = 0.8–1.0 GW/m^2; pulse duration $\tau = 4 \times 10^{-3}$ s. A change in the degree of laser spots overlapping was achieved by varying the pulse repetition frequency [51]. For all treatments, the structure over the entire depth of the laser melting zone (180–200 μm) remained practically uniform.

In the initial state, the sample was two-phase: the reflections from the α-titanium h.c.p.-lattice and a small amount of the β-titanium cubic lattice were observed by the XRD method (Fig. 10, *a*).

After LT, only reflections from the α-phase lattice were recorded in an argon atmosphere (Fig. 10, *b*). The absence of the β-phase in the surface layers is caused, as in the case of the LT of the VT-6 alloy, by the samples' rapid cooling with the implementation of diffusion-free martensitic $\beta \rightarrow \alpha'$-

transformation and the stabilization of the α-phase by α-Ti alloying elements dissolved in the lattice.

The α′-phase, which is formed in low-alloyed titanium alloys as a result of martensitic transformation, is a supersaturated solid solution of alloying elements in α-titanium [43]. It has a hexagonal lattice and is typical for martensite needle structure. Precise measurements of the α-phase lattice parameters showed their decrease compared to the original ones (Table 7). This can be explained by the fact that as a result of the $\beta \rightarrow \alpha'$-transformation, a supersaturated substitution solid solution of molybdenum in the α-Ti lattice is formed. Since the molybdenum atomic radii are smaller than the titanium atomic radius, the α-phase lattice parameters will also decrease after this treatment.

LT of the samples in a nitrogen atmosphere led to the formation of three phases in the melting zone: α-solid solution, TiN nitride, and a small amount of β-titanium (Fig. 10, *c*). The presence of some β-phase can be explained as follows. The melting zone is heterogeneous in chemical composition. Therefore, only two phases, α-Ti and TiN nitride, could form in the areas highly enriched with nitrogen, the β-phase, according to the Ti–N state diagram, was not formed at all, since nitrogen is an effective stabilizer of the α-phase [44, 52]. In regions with a smaller amount of nitrogen, the β-phase formation may have occurred first, followed by its disintegration by the monotectoid mechanism and the molybdenum-stabilized b.c.c. β-phase and the α-Ti phase formation. Since the XRD method is capable of determining the phase composition integral picture of the

Table 7. **Parameters of the VT-8 alloy α-Ti lattice after laser treatment in different atmospheres [51]**

Initial state	LT in an argon atmosphere	LT in the air atmosphere	LT in a nitrogen atmosphere
Lattice parameters, nm			
$a = 0.29323 \pm 0.00001$ $c = 0.46807 \pm 0.00009$	$a = 0.29313 \pm 0.00008$ $c = 0.46738 \pm 0.00009$	$a = 0.29501 \pm 0.00008$ $c = 0.47179 \pm 0.00019$	$a = 0.29501 \pm 0.00008$ $c = 0.47394 \pm 0.00019$

Table 8. **Phase composition and surface microhardness of the VT-8 alloy after LT in different gas atmospheres [51]**

Treatment type	Phase composition	Surface microhardness, GPa
Initial state	α-Ti, β-Ti	$H_\mu = 2.99 \pm 0.02$
LT in Ar atmosphere	α-Ti	$H_\mu = 5.62 \pm 0.04$
LT in N_2 atmosphere	α-Ti, β-Ti, TiN	$H_\mu = 7.82 \pm 0.18$
LT in the air atmosphere	α-Ti, β-Ti, TiN, TiO_2	$H_\mu = 6.56 \pm 0.09$

surface layers on depths up to 25–30 microns, the specified three phases were observed.

Lattice parameters of the titanium α-phase increased after LT in a nitrogen atmosphere (Table 7). This fact can be explained by the following considerations. The solubility of nitrogen in α-titanium at room temperature is about 3 at.%, and at high temperatures it can reach 22 at.% [41]. The melt cooling rate during LT is of about 10^4 K/s [37]. This makes it possible to obtain a supersaturated solid solution of nitrogen in the α-Ti lattice at room temperature, which was evidently the reason for the lattice parameters growth.

Note that, with this type of surface heat treatment, two competing processes could occur. Firstly, molybdenum, aluminium, and iron atoms could replace titanium atoms, which would lead to a decrease in the crystal lattice parameters. Secondly, a certain N atoms amount could be interstitial in the octahedral pores of the hexagonal lattice, which would lead to an increase in its parameters. It is obvious that, in our case, the formation of an interstitial solid solution had a more effect on changes in lattice parameters, which led to some increase in them.

During laser melting of the sample surface in an air atmosphere, four phases were observed in the alloy structure: α-Ti, TiN nitride, tetragonal TiO_2 oxide, and a small amount of β-Ti (Fig. 10, *d*). At the same time, an increase in α-Ti lattice parameters was also observed (Table 7). Note that, according to Ref. [40], in the Ti–O system, the solubility of oxygen in α-titanium at room temperature is 10 at.%, and at high temperatures, it is ≈35 at.%. Thus, as a result of melt rapid cooling during LT, at room temperature, a supersaturated solid solution of atmospheric gases (O and N) in the titanium lattice can form, which was the reason for the further increase in the α-phase lattice parameters.

After LT in all investigated atmospheres (Table 8), the microhardness of the samples' surface layers increased compared to the initial state. The change in microhardness values after LT in an argon atmosphere is associated with two competing factors: a small amount of the β-phase in the initial state, when the martensitic nature of the $\beta \rightarrow \alpha'$-transformation did not have a decisive effect on the weakening (as in the case of the VT-6 alloy), and an increase in the dispersion degree of the structure (dominant factor).

The increase in microhardness after LT in the atmosphere of nitrogen and air is also explained by the influence of several factors: the martensitic nature of the $\beta \rightarrow \alpha'$-transformation, the increase in the dispersion degree of the structure, solid-solution hardening due to the interstitial O and N atoms into the h.c.p.-lattice of titanium, and the formation of dispersed cubic titanium nitride.

It should be noted that the microhardness values of the alloy after LT in an air atmosphere were somewhat lower compared to the values after laser melting in a nitrogen atmosphere. The reason is that the amount of high-

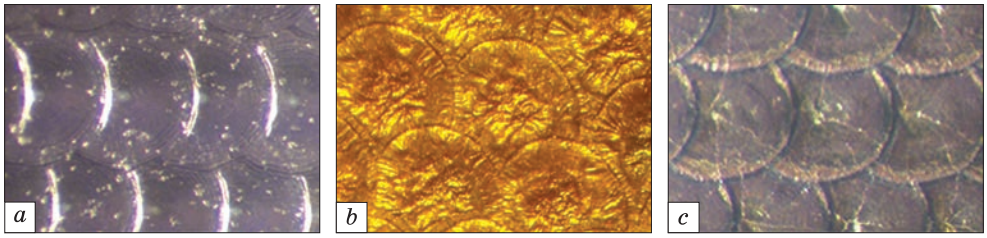

Fig. 11. Surface macrostructure of the VT-8 alloy after laser melting in an environment of argon (*a*), nitrogen (*b*) and air (*c*) [51]

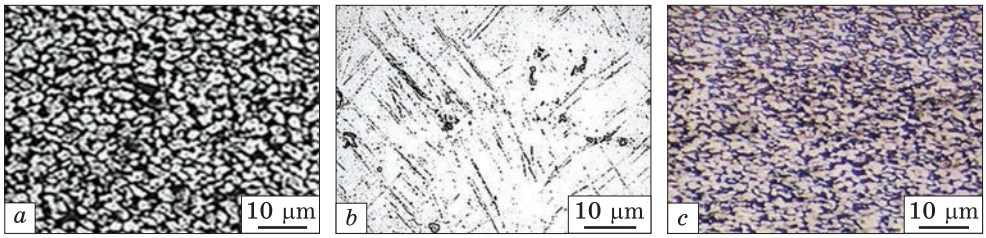

Fig. 12. The structure of the initial VT-8 alloy (*a*) and the surface layers of the laser melting zone cross section in an environment of argon (*b*) and nitrogen (*c*) [51]

strength TiN nitride after LT in a nitrogen atmosphere was higher. This ultimately led to an increase in the integral microhardness of the melted surface.

The appearance of surfaces melted in different gas environments had significant differences [51]. Thus, treatment in an argon environment (Fig. 11, *a*) led to the formation of laser spots with an almost mirror-like surface. A more or less contrasting spots image could be observed only under lateral illumination. At the same time, a weak relief in the form of concentric circles was detected on the spots surface, which was observed earlier in Ref. [53].

A significant amount of titanium nitride in the laser melting zone after treatment in a nitrogen atmosphere determined the golden colour of the laser-spots surface and the formation of a developed relief (Fig. 11, *b*) caused by the fact that TiN nitride is a refractory compound, and the formation of the surface macrostructure occurred very quickly, practically during the radiation pulse action ($\tau = 4 \cdot 10^{-3}$ s), which prevented surface tension forces from smoothing the laser-spot surface.

A characteristic feature of the spots after melting in the air atmosphere was the absence of a shiny surface and the presence of light areas in the spots peripheral areas. It can be explained by the fact that, at high temperatures, the refractory TiN nitride was first formed, and, according to [54], the TiN phase actively reacts with oxygen at high temperatures. Then, when the temperature drops to the temperature of TiO_2 oxide existence (<2133 K [40]), nitride oxidation begins with the formation of an

oxide film on the surface. The presence of light-coloured areas on the spot periphery is explained by the influence of two factors: firstly, the lower temperature in these areas due to the Gaussian energy distribution over the spot surface and, secondly, the higher melt cooling rates, which did not allow the process to go through sufficient oxidation. That is, the light areas can be identified as a mixture of nitride and oxide.

According to the metallographic analysis data, in the initial state, the α-Ti and β-Ti grain sizes were about 3 and 1.5 μm, respectively (Fig. 12, *a*).

LT in an argon atmosphere (Fig. 12, *b*) led to a change in the structure: in the cross-section of the laser-melting zone, the acicular structural components, characteristic of the α′-phase, were observed, *i.e.*, the martensitic nature of the β→α′-transformation was confirmed.

Metallographic studies of the sample after LT in a nitrogen atmosphere (Fig. 12, *c*) made it possible to observe an increase in the dispersion degree of the structure in comparison with the original one. It was not possible to detect the nitrides' inclusion using optical metallographic analysis.

Thus, the LT of the VT-8 alloy due to the high cooling rates of the melt leads to significant structural changes in the laser-melting zone, which, in turn, affects the microhardness growth of the samples' surface layers.

3.2. Laser Treatment of the VT1-0 Alloy Obtained by the Powder Metallurgy Method

The production of titanium and its alloys by traditional methods is a rather complex and expensive process. Therefore, to improve the manufacturability of titanium alloys production and to reduce the production cost, to obtain parts of a certain purpose, the powder metallurgy method is widely used, the advantages and features of which are given in Refs. [55–59].

According to the mentioned references, sintered titanium alloys have a lower density than cast ones, since they contain about 3–7% of pores by volume. If such materials are used as friction contact pairs, the pores on the surface can lead to leaks in the places of sealing, for example, in the manufacture of shut-off valves, as well as to the appearance of microregions with increased corrosion. Therefore, the question of minimizing the porosity of such alloys and increasing the wear resistance of their surface layers is relevant.

One of the ways to solve comprehensively the mentioned problems can be the surface laser treatment of sintered powder titanium alloy, the advantages of which are its locality and high manufacturability. This allows for non-contact surface treatment directly in the places where the friction pairs meet.

Surface laser treatment was performed in an argon atmosphere with a radiation power density of q = 900 MW/m^2 (surface melting mode) and with a pulse repetition frequency of 4 Hz and 20 Hz. The last treatment can be identified as continuous laser treatment. Thermomechanical titanium powders of PT5-1 grade, fraction –0.50/+0.16, composition VT1-0

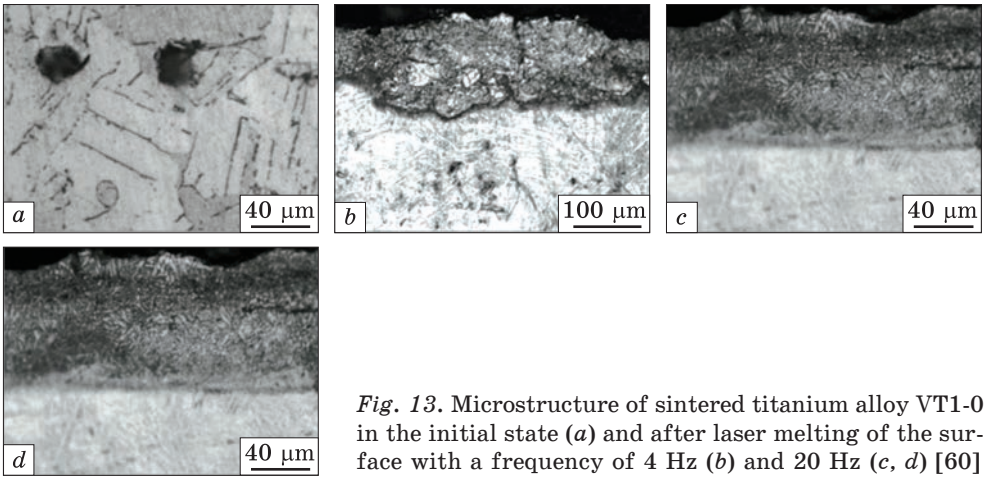

Fig. 13. Microstructure of sintered titanium alloy VT1-0 in the initial state (*a*) and after laser melting of the surface with a frequency of 4 Hz (*b*) and 20 Hz (*c*, *d*) [60]

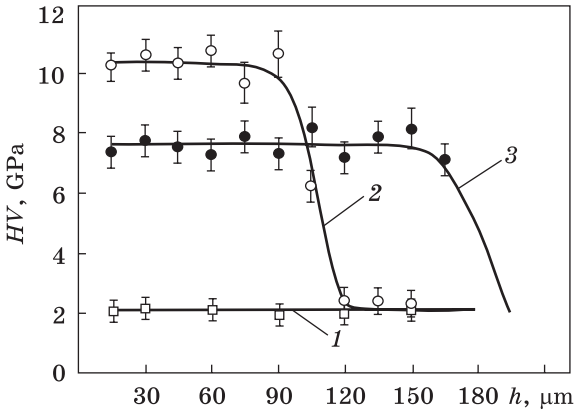

Fig. 14. Microhardness distribution of sintered titanium alloy VT1-0 by the thickness of the laser-melting zone: *1* — initial state; *2* and *3* — after laser melting with frequencies of 4 Hz and 20 Hz, respectively [60]

were chosen as the starting material. Alloys were formed by batch pressing on a hydraulic press with a pressure of 700 MPa. The obtained blanks were subjected to sintering according to the scheme: vacuum heating to 1523 K + exposure for 180 min + cooling with a furnace [60].

No noticeable changes in the crystal structure after LT were deteced by the x-ray method: the XRD patterns were almost identical to those obtained during LT of the VT1-0 cast alloy (Fig. 1, *a*, *b*). Some redistribution of the diffraction maxima intensities after LT indicated a slight texturing of the surface layers caused by directed heat removal into the matrix during auto-quenching of the melt bath.

Metallographic studies revealed several morphological features of the melting zone (Fig. 13). Thus, in the initial state, pores with a size of 10–20 μm were observed throughout the entire sample volume (Fig. 13, *a*). LT with a frequency of 4 Hz led to the formation of a structure in the melting zone that practically did not contain pores. The sizes of the pores

small number that were still fixed were significantly smaller than the pores sizes in the initial state and were about 2–3 μm (Fig. 13, *b*). The decrease in the pores' size and their total number can be explained by the conditions of melt solidification: pulsed laser melting led not only to an intensive heat supply to the laser influence zone but also to an intensive melt component mixing in it (Marangoni–Gibbs effect). Such mixing in combination with high rates of material heating and cooling were, obviously, the main reasons for the formation of the obtained structure. It should be noted that increasing the frequency to 20 Hz caused the formation of a more uniform structure in the melting zone. At the same time, the zone depth increased (Fig. 13, *c, d*).

A sharp increase in the level of structure dispersion, which was accompanied by a significant increase in the grain boundaries' overall length, had a significant effect on the surface layers' mechanical properties. In this connection, the changes in the microhardness integral values by the melting zone thickness were investigated. It was established that the microhardness in the treated samples melting zone was several times higher than the initial one (Fig. 14).

The nature of the change in the microhardness curves for samples treated in both frequency regimes was identical and typical for single-phase laser melting zones. However, treatment with a higher frequency, which led to an increase in the LAZ depth, caused a slight decrease in the microhardness values. This can be explained by a change in treatment conditions: with increasing frequency, the amount of energy supplied to the treated surface of the sample increased, which became the reason for the increase in the LAZ thickness. At the same time, such an increase in the amount of energy led to the fact that the melt cooling rate decreased somewhat, which could affect both the overall size and the morphological features of the LAZ structural components.

All samples were melted by a laser in an argon flow; so, the possibility of melt saturation with atmospheric gases during treatment was minimized. In other words, the formation of a solid solution of nitrogen and oxygen in the titanium h.c.p.-lattice, which could affect the LAZ strengthening, was practically excluded, since the lattice parameters of the studied alloy after various treatments practically did not change and did not differ from the initial ones. It is obvious that, in this case, the main reason for a significant increase in microhardness could be only an increase in the dispersion degree of the structural components.

3.3. VT25U Alloy Complex Treatment

Increasing the titanium alloys strength by traditional methods, *i.e.*, alloying or thermomechanical treatments, is quite limited and is practically exhausted today. Among the technologies for strengthening the surfaces of parts

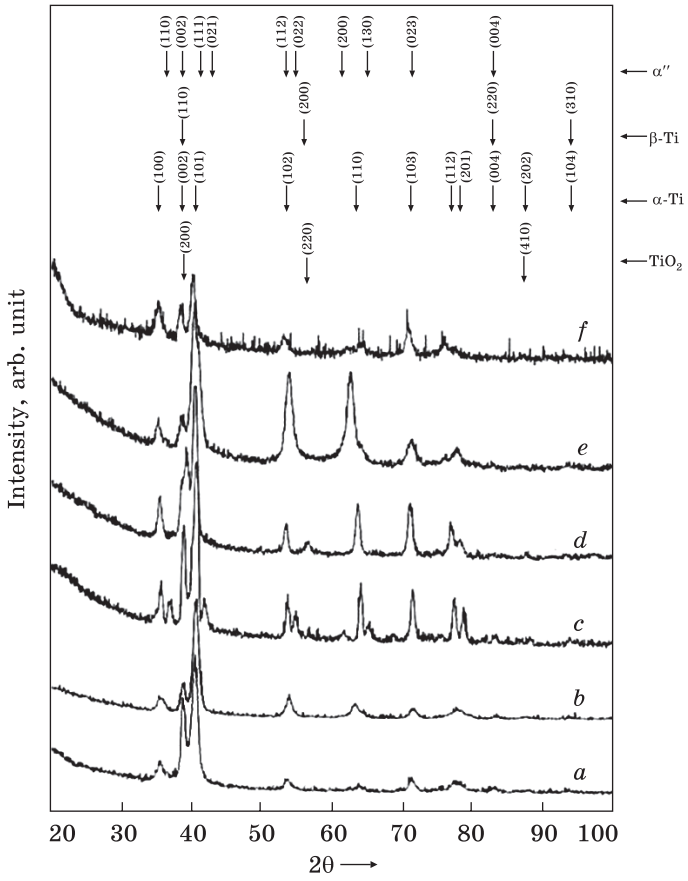

Fig. 15. XRD-patterns from the surface of VT25U alloy samples: (*a*) initial state; (*b*) initial state + LT; (*c*) quenching; (*d*) quenching + + twist extrusion; (*e*) quenching + twist extrusion + LT (q_1 = 0.86 GW/m^2); (*f*) quenching + twist extrusion + LT (q_1 = 1.20 GW/m^2) [64]

Table 9. **Phase composition of the studied samples [64]**

Sample No.	Treatment type	Phase composition
1	initial state	α-phase, β-phase
2	initial state + LT	α-phase, α″-phase
3	initial state + quenching	α-phase, α″-phase
4	quenching + twist extrusion	α-phase, α″-phase, TiO_2 oxide
5	quenching + twist extrusion + + LT (q_1 = 0.86 GW/m^2)	α-phase, α″-phase
6	quenching + twist extrusion + + LT (q_1 = 1.20 GW/m^2)	α-phase, α″-phase
7	annealing + twist extrusion	α-phase, α″-phase, β-phase, TiO_2 oxide
8	annealing + twist extrusion + + LT (q_1 = 0.86 GW/m^2)	α-phase, α″-phase
9	annealing + twist extrusion + + LT (q_1 = 1.20 GW/m^2)	α-phase, α″-phase

made of titanium alloys, for example, parts of gas turbine engines, the technology of ultrasonic strengthening and surface plastic deformation has become widespread [61]. However, the temperature range of application for such hardening is limited by the temperatures of the recrystallization beginning.

Fairly new methods for increasing the strength of structural materials are technologies based on intensive plastic deformation and allowing obtaining structures of nano- and submicrocrystalline sizes. Among such technologies, twist extrusion, which consists in repeatedly pushing blanks through the screw matrix channel, deserves special attention. At the same time, the initial shapes and sizes of the workpieces are preserved [62].

Strengthening the surface of titanium parts remains a separate issue, since the surface properties determine the service life of the part. In this regard, the use of twist extrusion technology followed by laser treatment can become an effective method of surface strengthening. For complex alloyed heat-resistant titanium alloys, like VT25U, with an operating temperature of up to 820 K, which are used, for example, for highly loaded rotor parts of gas turbine engines [63], such treatment was not investigated.

Laser treatment of VT25U alloy samples after twist extrusion was performed in a protective argon environment at radiation power densities $q_1 = 0.86$ GW/m^2 and $q_2 = 1.20$ GW/m^2 [64].

According to the XRD data, the alloy was two-phase in its initial state (sample No. 1, Table 9): reflections from the h.c.p. lattice of α-phase and the b.c.c. lattice of β-phase were observed on the XRD-patterns (Fig. 15, *a*). Note that, during intense plastic deformation, the β-phase can break up into martensitic-type phases.

After quenching from the initial state (sample No. 3) as a result of melt rapid cooling, two phases were detected in the alloy structure: titanium α-phase and martensitic type α″-phase (Fig. 15, *c*). XRD-studies of sample No. 4 showed the presence of α-phase, α″-phase and TiO_2 oxide traces in the alloy (Fig. 15, *d*).

The twist extrusion application to the annealed sample (sample No. 7) made it possible to record reflections from α-phase lattices, a small amount of β-phase, α″-phase and TiO_2 oxide traces on XRD-patterns (Fig. 16, *c*). At the same time, the martensitic transformation was not completed to the end, as a certain reflections number from the β-phase were observed. The reason for the incomplete $\beta \rightarrow \alpha''$ transformation according to the martensitic type may be the presence of a significant number of defects in the crystal structure after twist extrusion [65].

Samples Nos. 2, 5, 6, 8, and 9 were subjected to laser treatment (Table 9). During surface laser melting, the high-temperature β-phase in the crystallization process can have concentration gradients due to the heterogeneous nature of the melt mixing under the influence of hydrodynamic flows arising in the LAZ. The chemical heterogeneity of the β-phase together with high cooling rates of the melt (~10^4 K/s [37]) can create condi-

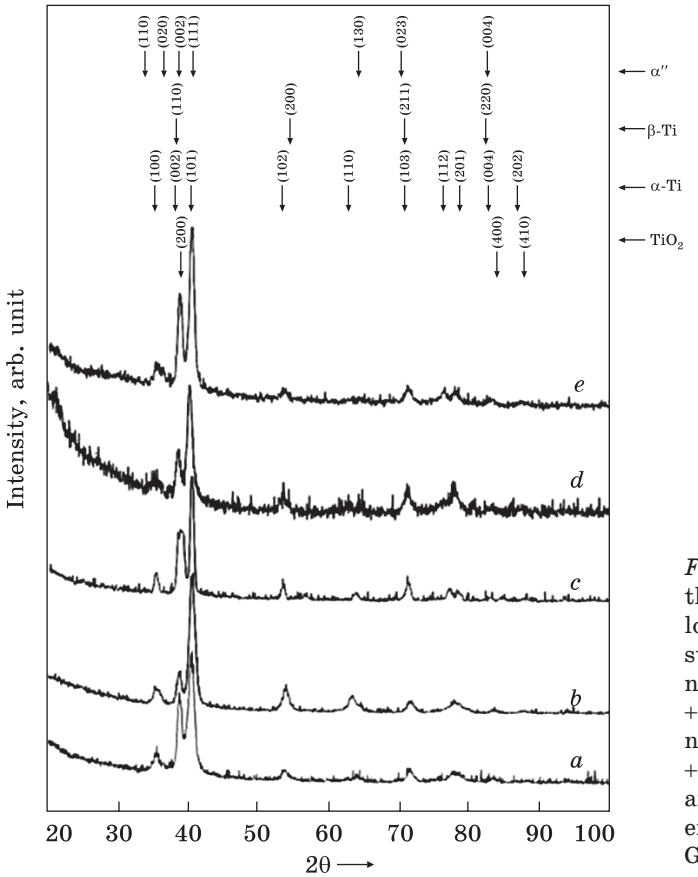

Fig. 16. XRD-patterns from the surface of VT25U alloy samples for (*a*) initial state, (*b*) initial state + annealing, (*c*) annealing + + twist extrusion, (*d*) annealing + twist extrusion + + LT (q_1 = 0.86 GW/m^2), and (*e*) annealing + twist extrusion + LT (q_1 = 1.20 GW/m^2) [64]

tions for the metastable martensitic-phases' formation. Indeed, all samples after LT had a two-phase structure: on XRD-patterns were detected reflections only from the lattices of the α-phase and α″-martensite (Figs. 15, 16). No traces of β-phase presence were observed within the method sensitivity.

The formation of the martensitic-type α″-phase occurs mainly in complex alloys, which include the VT25U alloy [66]. The martensitic α″-phase has an orthorhombic crystal lattice, which is a distortion of the α-titanium hexagonal lattice and is formed as a result of α-solid solution supersaturation with alloying elements. Martensite in titanium alloys has its characteristic features and differs from classic martensite, for example, in carbon steel, because martensite in steels is a supersaturated solid solution of carbon in α-iron, and martensite in titanium alloys is a substitutional solid solution of alloying elements in α-titanium. Therefore, in the case of martensitic β→α″-transformation in titanium alloys, a relatively weak strengthening effect is observed due to a slight lattice distortion, and the α″-phase is more ductile than the α-phase. In this regard, it can be assumed that the plastic α″-phase formation led to a certain decrease in the internal

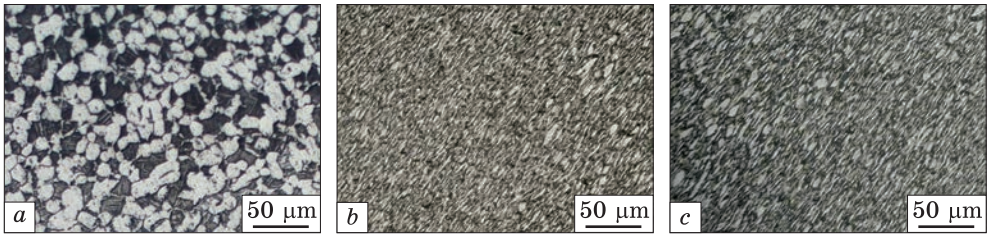

Fig. 17. Microstructure of the VT25U alloy in its initial state (*a*) and after helical extrusion of pre-quenched (*b*) and pre-annealed samples (*c*) [64]

stresses in the alloy, which increased sharply during the twist extrusion process. This obviously was the reason why the material after such treatment did not have small macrodefects such as pores and microcracks.

One of the XRD-patterns features after LT was the redistribution of the diffraction maxima intensities compared to the samples to which LT was not applied. Such changes in the XRD patterns indicated the crystalline texture presence, the appearance of which was caused by directed heat removal during laser-melting zones' rapid cooling.

Thus, laser treatment of the VT25U alloy made it possible to obtain the metastable α″-phase, which is more plastic than the α-phase, and the formation of which should lead to some internal stresses relaxation in the alloy after extrusion.

Metallographic analysis of the samples was carried out to clarify the XRD-data. In its initial state, the VT25U alloy was two-phase. The sizes of the α- and β-phase grains were of about 10–15 μm (Fig. 17, *a*).

Twist extrusion of the sample quenched from the two-phase region (sample No. 4) led to the grinding of its structure. Immediately after quenching the structure was a mixture of primary α-phase grains and a small number of α″-phase grains (10–15 μm in size). After extrusion, the dispersion degree increased noticeably — the grain sizes did not exceed 2 μm for both phases (Fig. 17, *b*). Extrusion of a pre-annealed sample (sample No. 7) led to the formation of a similar structure (Fig. 17, *c*).

LT of samples in their initial state (sample No. 2) and after various treatment types (samples Nos. 5, 6, 8, and 9) with different radiation power densities made it possible to obtain a highly dispersed structure in the melting zone, which was very weakly amenable to etching by standard etchants for titanium alloys. Therefore, it turned out to be impossible to interpret unambiguously the structure using the optical metallography methods. It was possible to determine the structural-components' average size only with a certain percentage of probability: it did not exceed 1 μm. Such grains' size became the determining factor affecting the increased corrosion resistance of the melting zone, but this cannot be stated unequivocally, since separate studies are required.

The change in the samples' mechanical properties after various types of treatments was monitored by measuring the microhardness average values (H_μ), which were different before conducting the LT: in the initial state, H_μ = 3.29 GPa; after quenching and subsequent twist extrusion, H_μ = 4.07 GPa; and after annealing and subsequent twist extrusion, H_μ = 3.76 GPa. LT of samples after such treatments led to some increase in H_μ values, which turned out to be approximately the same and amounted to 4.27, 4.24, and 4.26 GPa, respectively. The reason for such a change in the microhardness of the alloy surface layers as a result of the LT can be mainly two factors: (i) the martensitic α″-phase formation and (ii) a decrease in the structural components size, which leads to an increase in the two-dimensional defects total number (grain boundaries), which is an effective barrier for the movement of the dislocations in metal alloys.

It should be noted that the effect of VT25U alloy strengthening by means of laser treatment compared to others, such as aluminium alloys [67–69], was much lower. The reason lies in the different effects of the above-mentioned factors on the alloy strengthening; if the increase in the dispersion degree leads to the LAZ strengthening, then, the martensitic α″-phase formation, which is more plastic than the α-phase, causes a decrease in the microhardness values. In our case, the role of the second factor was greater, as evidenced by a slight increase in the H_μ average values.

Comparing the H_μ values for the samples subjected to twist extrusion (both after pre-quenching and pre-annealing) with the values after LT of the original sample, it is easy to see that the latter are slightly higher. In other words, if the surface properties of the parts are of decisive importance in case of products operation made of VT25U alloy, the use of high-energy preliminary heat treatments and extrusion is impractical.

3.4. Laser Alloying

The use of laser alloying of metal-alloy surfaces to obtain coatings with special properties allows significant expanding the Ti-based alloys application scope, as it can lead to the formation of fundamentally new structural states in the surface layer that cannot be obtained by other methods. In particular, titanium alloying with iron-group transition metals (TM) can lead, under certain concentration and temperature conditions, even to the quasi-crystalline structures formation [70]. Therefore, the study of the titanium samples' surface layers structure during laser alloying with powders, for example, iron, cobalt, and nickel, can be of not only theoretical but also practical interest.

Industrial alloy VT1-0 was used as the object of research. Alloying was carried out by the coating method (binder is BF-6 glue) in a protective argon environment with 30% laser spots overlapping. Pure elements powders of Fe, Co, and Ni with a fraction size of no more than 50 μm served

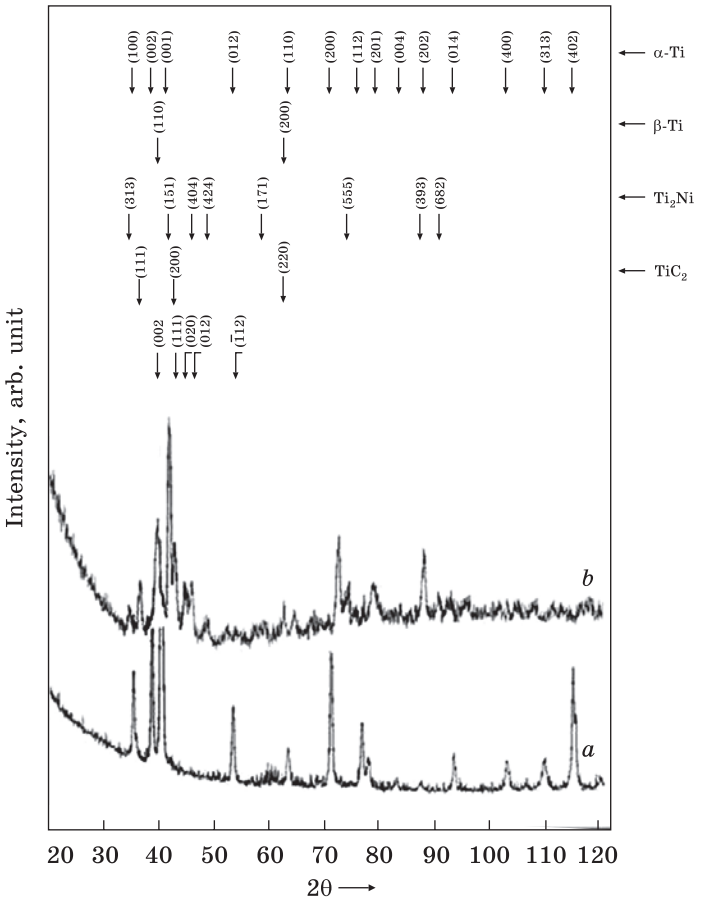

Fig. 18. XRD-patterns from the VT1-0 alloy in its initial state (*a*) and after laser alloying with nickel (*b*) [64]

as alloying components. The back-coat thickness was about 150 μm. The alloyed zone depth was 200 μm.

In the initial state, the samples were single-phase: only reflections from the α-Ti lattice were observed on the XRD patterns (Fig. 18, *a*). The samples' surface layers alloyed with nickel had the most complex phase composition. Reflections from the lattices of the following phases were detected: β-Ti-based solid solution, TiNi intermetallic with a monoclinic lattice, Ti_2Ni intermetallic with an FCC lattice, and TiC-type cubic carbide (Fig. 18, *b*) [71].

After alloying titanium samples with cobalt, the phase composition was as follows: a solid solution based on β-Ti, TiC carbide, and traces of TiCo cubic intermetallide (Fig. 19, *a*). Alloying with iron led to the formation of only two phases in the laser-alloying zone: a solid solution based on β-Ti and TiC carbide (Fig. 19, *b*).

The absence of reflections from the α-Ti lattice on all XRD patterns can be due to several reasons. First, high cooling rates during pulsed laser alloying led to significant melt undercooling, which in conditions of non-

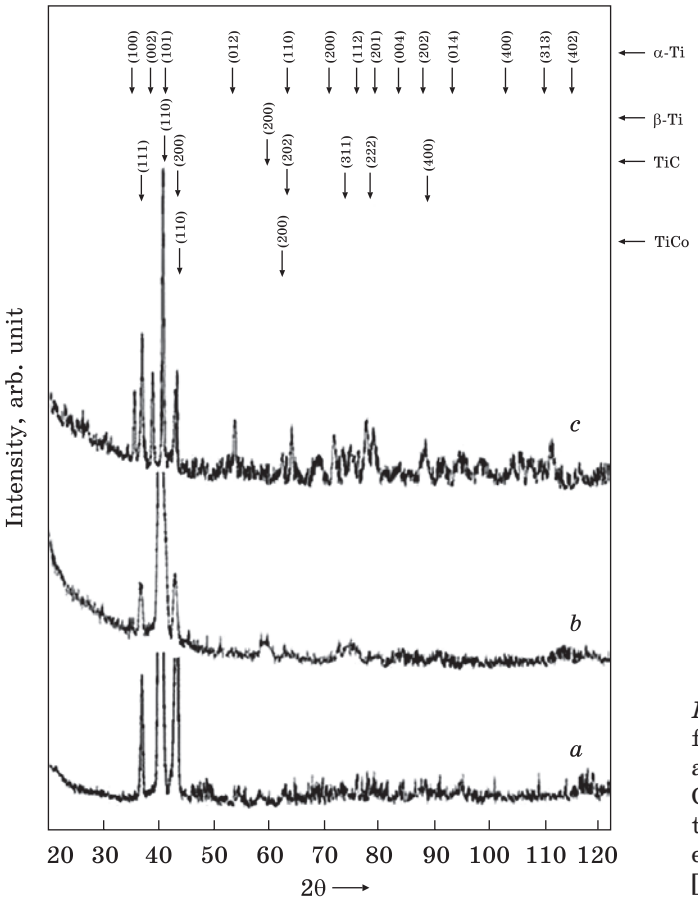

Fig. 19. XRD-patterns from the VT1-0 alloy but after laser alloying with Co (*a*), Fe (*b*), and laser treatment of samples covered with glue layer (*c*) [64]

equilibrium crystallization can significantly lower the polymorphic β→α-transformation temperature. Secondly, iron group transition metals (Fe, Ni, Co) are quite strong stabilizers of the titanium β-phase. In our opinion, the complex influence of these factors led to the fact that the α-Ti phase was absent in the laser alloying zone.

The highest solubility in β-Ti possesses iron (22%) followed by cobalt (14.5%) and nickel (8%) [72]. Assume that the concentration of alloying components in the laser alloying zone in all cases is approximately the same and exceeds 22%, and the cooling rate is also equally high (10^4 K/s) [37]. Then, such phase formation conditions should lead to the fact that the intermetallics content in the laser-alloying zone should have a definite dependence on the components' solubility in the β-phase. This assumption explains the fact that, during laser alloying with iron, not even traces of intermetallics were detected by the method.

In the case of alloying with cobalt, as a result of the mentioned reason, together with the β-solid solution of cobalt in titanium, traces of the cubic

intermetallide TiCo were also detected. The β-phase content during alloying with nickel was even lower. In this regard, in the process of alloying titanium with nickel, a rather complex heterophase structure was formed, which included two intermetallics: monoclinic (TiNi) and f.c.c. (Ti_2Ni) lattices.

The TiNi b.c.c. phase undergoes a thermoelastic martensitic transformation under a certain deformation with the low-symmetric phase formation of the same stoichiometry [73]. Laser alloying as a result of high cooling rates of the melt leads to the occurrence of fairly significant quenching stresses in the laser-alloying zone [12], which can stimulate the specified transformation. Therefore, during alloying titanium with nickel in the laser-alloying zone, the formation of the intermetallic TiNi with a monoclinic, not cubic lattice took place, as in the case of alloying titanium with cobalt.

Consider the reason for the Ti_2PM type phase formation, which was observed in the laser-alloying zone only after alloying titanium with nickel. For this purpose, state diagrams of the three systems were analysed: Ti–Fe, Ti–Co, and Ti–Ni [72].

There is no Ti_2Fe type phase in the Ti–Fe diagram at all. In the Ti–Co system, the Ti_2Co phase is formed by a peritectic reaction in a fairly wide concentration range. In addition, the Ti_2Co phase has practically no homogeneity region. Then, due to the high cooling rates of the melt during quenching from the liquid state in the laser alloying process, the probability of the formation of such a phase will be very low. The Ti_2Ni phase has a narrower concentration interval of formation by the peritectic reaction and even some homogeneity region. In addition, stresses arising in the quenching process from the liquid state will be partially relaxed as a result of the martensitic transformation of the cubic intermetallic TiNi into a monoclinic one, thereby, facilitating the peritectic reaction process. This can explain the presence of a fairly significant amount of intermetallic Ti_2Ni in the laser-alloying zone.

Thus, despite the close physical and chemical properties of the alloying components, the alloying zone phase compositions have significant differences, which are determined both by the solubility degree of the used transition metals in the titanium β-phase and by the highly non-equilibrium structure formation conditions.

The TiC carbide formation, which is present in all cases, can be explained by the decomposition at high temperatures of the organic binder (BF-6 glue), which contains a significant amount of carbon, with its subsequent entry into the melt. To confirm this explanation, laser melting of the titanium sample surface covered only with a glue layer was performed. Indeed, along with the maxima from the α-Ti lattice, reflections from the lattice of cubic TiC carbide (Fig. 19, *c*) with the lattice parameter a = = 0.430 nm, which is slightly smaller than the table one (a = 0.433 nm), were also detected on the XRD-patterns. Such a difference may be due to the formation of not pure titanium carbide, but a Ti(C,N)-type solution.

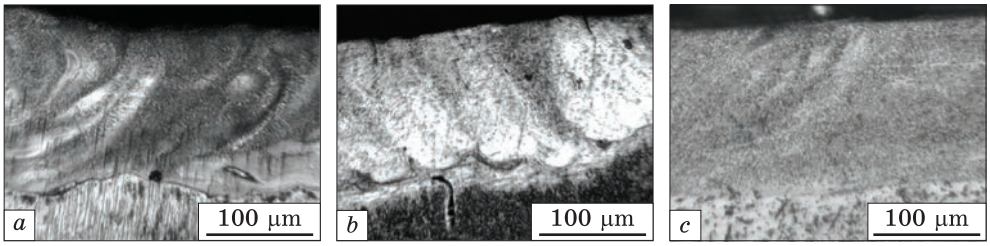

Fig. 20. Cross-sectional structure of the laser alloying zone of titanium samples with nickel (*a*), iron (*b*) and cobalt (*c*) [71]

No reflections from the β-phase lattice were observed. This suggests that the determining factor in the laser alloying zone structure formation was not the melt cooling rate, but alloying of it with transition metals.

Metallographically, after all types of alloying, a dispersed structure was observed (Fig. 20). The structural components' sizes did not exceed 2–3 μm. It turned out to be practically impossible to determine the phase composition by this method, both due to the alloying zone heterogeneity in terms of chemical composition and due to the occurrence of Marangoni–Gibbs-type capillary effects within it.

The microhardness value in the samples' surface layers turned out to be maximal after alloying with iron and was about 14 GPa. After alloying with cobalt, the microhardness was 5–6 GPa, and with nickel, of 7 GPa. The microhardness of the samples' surface layers covered only with a glue layer (60 μm thick) after laser treatment was from 7 GPa to 9 GPa. It is obvious that a significant microhardness increase after alloying with iron group transition metals is primarily due to the titanium carbide formation, the microhardness of which reaches 30 GPa. Establishing the reason for the significant difference between the microhardness of the samples' surface layers alloyed with cobalt and nickel and samples alloyed with iron requires further research.

4. Conclusions

Pulsed laser treatment of titanium alloys due to high (~10^4 K/s) cooling rates of the melt leads to an increase in the dispersion degree of the laser melting zone and, as a result, to an increase in microhardness values.

The surrounding gas atmosphere and the titanium alloy chemical composition significantly affect the structure formation processes during their laser melting. The strength characteristics of the laser action zone can be determined by the complex action of several factors: an increase in the dispersion degree of structural components, the high-temperature metastable intermetallic phase formation, the completeness and character of the polymorphic β→α-transformation, the dispersed carbides and nitrides formation, and solid-solution strengthening.

Laser melting of the sintered single-phase powder titanium VT1-0-type alloy surface leads to a sharp decrease in porosity in the melting zone.

The microhardness in the VT25U alloy laser-melting zone exceeds the microhardness of samples after heat treatments and twist extrusion. Only mechanical properties of the material surface layers are important using products from this alloy, so laser melting of the initial material surface is more effective and technological than heat treatment or twist extrusion.

The formation of the Ti2TM type intermetallics during laser alloying of titanium with iron, cobalt, and nickel powders is determined by the solubility degree of the alloying components in β-phase, the concentration range of the intermetallide homogeneity and the high cooling rate of the melt.

REFERENCES

1. G.D. Revankar, R. Shetty, S.S. Rao, and V.N. Gaitonde, *J. Mater. Res. Technol.*, **6**, No. 1: 13 (2017); https://doi.org/10.1016/j.jmrt.2016.03.007
2. O.M. Ivasishin, P.E. Markovsky, S.L. Semiatin, and C.H. Ward, *Mater. Sci. Eng. A*, **405**, No. 1-2: 296 (2005); https://doi.org/10.1016/j.msea.2005.06.027
3. O.M. Ivasishin, P.E. Markovsky, Yu.V. Matviychuk, S.L. Semiatin, C.H. Ward, and S. Fox, *J. Alloys Comp.*, **457**, Nos. 1–2: 296 (2008); https://doi.org/10.1016/j.jallcom.2007.03.070
4. D. Kuroda, M. Niinomi, M. Morinaga, Y. Kato and T. Yashiro, *Mater. Sci. Eng. A*, **243**, Nos. 1–2: 244 (1998); https://doi.org/10.1016/S0921-5093(97)00808-3
5. T. Saito, T. Furuta, J.W. Hwang, S. Kuramoto, K. Nishino, N. Suzuki, R. Chen, A. Yamada, K. Ito, Y. Seno, T. Nonaka, H. Ikehata, N. Nagasako, C. Iwamoto, Y. Ikuhara, and T. Sakuma, *Science*, **300**, No. 5618: 464 (2003); https://doi.org/10.1126/science.1081957
6. M.A.H. Gepreel and M. Niinimi, *J. Mech. Behav. Biomed. Mater.*, **20**: 407 (2013); https://doi.org/10.1016/j.jmbbm.2012.11.014
7. M. Motyka, W. Ziaja, and J. Sieniawski, *Titanium Alloys — Novel Aspects of Their Manufacturing and Processing* (London: Intechopen: 2019), p. 154; https://doi.org/10.5772/intechopen.83722
8. A. Yamashita, D. Yamaguchi, Z. Horita, and T. G. Langdon, *Mater. Sci. Eng. A*, **287**, No. 1: 100 (2000); https://doi.org/10.1016/S0921-5093(00)00836-4
9. Y.G. Ko, D.Y. Hwang, D.H. Shin, S. Lee, and C. S. Lee, *Mater. Sci. Eng. A*, **493**, Nos. 1–2: 164 (2008); https://doi.org/10.1016/j.msea.2007.06.091
10. R. Lapovok, D. Tomus, and B.C. Muddle, *Mater. Sci. Eng. A*, **490**, Nos. 1–2: 171 (2008); https://doi.org/10.1016/j.msea.2008.01.075
11. H.P. Ng, C. Haase, R. Lapovok, and Y. Estrin, *Mater. Sci. Eng. A*, **565**: 369 (2013); https://doi.org/10.1016/j.msea.2012.12.071
12. V.S. Trush, I.M. Pohreliuk, and V.M. Fedirko, *Physical Metallurgy and Heat Treatment of Metals*, **94**, No. 3: 65 (2021); https://doi.org/10.30838/J.PMHTM.2413.010721.65.783
13. D. Nolan, S.W. Huang, V. Leskovsek, and S. Braun, *Surf. Coat. Technol.*, **200**, Nos. 20–21: 5698 (2006);

https://doi.org/10.1016/j.surfcoat.2005.08.110
14. I.M. Pohrelyuk, M.V. Kindrachuk, and S.M. Lavrys', *Physicochemical Mechanics of Materials*, No. 1: 56 (2016) (in Ukrainian).
15. A. Zhecheva, S. Malinov, and W. Sha, *Surf. Coat. Technol.*, **201**, No. 6: 2467 (2006); https://doi.org/10.1016/j.surfcoat.2006.04.019
16. K. Tokaji, T. Ogawa, and H. Shibata., *J. of Mater. Eng. Perform.*, **8**, No. 2: 159 (1999); https://doi.org/10.1361/105994999770346990
17. A. Zhecheva, W. Shaa, S. Malinov, and A. Long., *Surf. Coat. Technol.*, **200**, No. 7: 2192 (2005); https://doi.org/10.1016/j.surfcoat.2004.07.115
18. O. Tisov, M. Lepicka, Yu. Tsybrii, A. Yurchuk, M. Kindrachuk, and O. Dukhota, *Metals*, **12**, No. 1: 100 (2022); https://doi.org/10.3390/met12010100
19. S. Madhukar, P.V. Sai, S. Kumar, and D.J. Prakash, *Int. J. Curr. Eng. Technol.*, **7**, No. 1: 238 (2017).
20. A.F. Yetim, A. Alsaran, I. Efeoglu, and A. Celik, *Surf. Coat. Technol.*, **202**, No. 11: 2428 (2008); https://doi.org/10.1016/j.surfcoat.2007.08.027
21. D. Ferro, M. Barinov, J.V. Ran, A. Latini, R. Scandurra, and B. Brunetti, *Surf. Coat. Technol.*, **200**, No. 16: 4701 (2006); https://doi.org/1016/j.surfcoat.2005.02.150
22. D. Ferro, J.V. Rau, A. Generosi, V. Rossi Albertini, A. Latini, and S.M. Barinov, *Surf. Coat. Technol.*, **202**, No. 10: 2162 (2008); https://doi.org/10.1016/j.surfcoat.2007.09.008
23. Y.Y. Liu, Z.K. Yao, H.Z. Guo, and H.H. Yang, *Int. J. Min. Met. Mater.*, **16**, No. 5: 568 (2009); https://doi.org/10.1016/S1674-4799(09)60098-4
24. T. Mohandas, D. Banerjee, and V. V. Kutumbarao, *Mater. Sci. Eng. A*, **269**, Nos. 1–2: 217 (1999); http://doi.org/10.1016/S0921-5093(99)00172-0
25. V.P. Rotshtein, D.I. Proskurovsky, G.E. Ozur, Yu.F. Ivanov, and A.B. Markov, *Surf. Coat. Technol.*, **180–181**: 377 (2004); https://doi.org/10.1016/j.surfcoat.2003.10.085
26. D. Utu, G. Marginean, C. Pogan, W. Brandi, and V A. Serban, *Surf. Coat. Technol.*, **201**, No. 14: 6387 (2007); https://doi.org/10.1016/j.surfcoat.2006.12.012
27. V.F. Bashev, O.E. Beletskaya, N.A. Korovina, N.A. Kutseva, and A.A. Lysenko, *Phys. Chem. Solid State*, **6**, No. 1: 141 (2005) (in Ukrainian).
28. B. Courant, J.J. Hantzpergue, L. Avril, and S. Benayoun, *J. Mater. Proces. Technol.*, **160**, No. 3: 374 (2005); https://doi.org/10.1016/j.jmatprotec.2004.06.025
29. Y. Tian, C. Chen, S. Li, and Q. Huo, *Appl. Surf. Sci.*, **242**, Nos. 1–2: 177 (2005); https://doi.org/10.1016/j.apsusc.2004.08.011
30. G. Luo, G. Wu, Z. Huang, and Z. Ruan, *Mater. Charact.*, **60**, No. 6: 525 (2009); https://doi.org/10.1016/j.matchar.2008.12.009
31. A. Poulon-Quintin, I. Watanabe, E. Watanabe, and C. Bertrand, *Dent. Mater.*, **28**, No. 9: 945 (2012); https://doi.org/10.1016/j.dental.2012.04.008
32. Q. Qiao, V.A.M. Cristino, L.M. Tam, and C.T. Kwok, *Surf. Coat. Technol.*, **458**: 129357 (2023); https://doi.org/10.1016/j.surfcoat.2023.129357

33. Z. D. Liu, X.C. Zhang, F.Z. Xuan, Z.D. Wang, and S.T. Tu, *Mater. Design*, **37**: 268 (2012); https://doi.org/10.1016/j.matdes.2011.12.008
34. X.B. Liu, X.J. Meng, H.Q. Liu, G.L. Shi, S.H. Wu, C.F. Sun, M.D. Wang, and L.H. Qi, *Mater. Design.*, **55**: 404 (2014); https://doi.org/10.1016/j.matdes.2013.09.038
35. B. Ruiliang, Y. Huijun, C. Chuanzhong, Q. Biao, and Z. Lijian, *Surf. Rev. Lett.*, **13**, No. 5: 645 (2006); https://doi.org/10.1142/S0218625X06008608
36. B.F. Mohazzab, B. Jaleh, A. Fattah-alhosseini, F. Mahmoudi and A. Momeni, *Surfaces and Interfaces*, **20**, 100597 (2020); https://doi.org/10.1016/j.surfin.2020.100597
37. D.I. Anpilogov and V.V. Girzhon, *Ukr. J. Phys.*, **3**, No. 42: 301 (1997) (in Ukrainian).
38. R. Filip, *J. Achiev. Mater. Manuf. Eng.*, **15**, No. 2: 174 (2006).
39. V.V. Girzhon, V.V. Yemelianchenko, O.V. Kushch, and I.O. Bykov, *Metallofiz. Noveishie Tekhnol.*, **42**, No. 4: 553 (2020) (in Ukrainian); https://doi.org/10.15407/mfint.42.04.0553
40. H. Okamoto, *J. Phase Equilib. Diffus.*, **32**: 473 (2011); https://doi.org/10.1007/s11669-011-9935-5
41. H. Okamoto, *J. Phase Equilib. Diffus.*, **34**: 151 (2013); https://doi.org/10.1007/s11669-012-0153-6
42. V.V. Girzhon and O.V. Kushch, *Sposib Zmitsnennya Detalei z Legovanoho Tytanovoho Splavu* [Method of Strengthening Details Made from Alloyed Titanium Alloy] (2021) (in Ukrainian); https://web.znu.edu.ua/NIS/2021/getdocument__7_.pdf
43. X. Chen, G. Wu, R. Wang, W. Guo, J. Yang, S. Cao, Y. Wang, and W. Han, *Surf. Coat.Tech.*, **201**, Nos. 9–11: 4843 (2007); https://doi.org/10.1016/j.surfcoat.2006.07.186
44. U. Zwicker, *Titan und Titanlegierungen* (Heidelberg: Springer Berlin: 2013); https://doi.org/10.1007/978-3-642-80587-5
45. S. Gokul Lakshmi, D. Arivuoli, and B. Ganguli, *Mater. Chem. Phys.*, **76**, No. 2: 187 (2002); https://doi.org/10.1016/S0254-0584(01)00517-X
46. A.S. Gornakova, B.B. Straumal, and S.I. Prokofiev, *Adv. Eng. Mater.*, **2018**, 1800510 (2018); https://doi.org/10.1002/adem.201800510
47. M. Sujata, M. Madan, K. Raghavendra, and S.K. Bhaumik, *Procedia Eng.*, **55**: 481 (2013); https://doi.org/10.1016/j.proeng.2013.03.284
48. *Titanium and Titanium Alloys: Fundamentals and Applications* (Eds. C. Leyens and M. Peters) (Weinheim: Wiley-VCH Verlag GmbH & Co. KGaA: 2003); https://doi.org/10.1002/3527602119
49. C. Carson, *Heat Treating of Titanium and Titanium Alloys* (Eds. G.E. Totten) (ASM International: 2016), p. 511; https://doi.org/10.31399/asm.hb.v04e.a0006283
50. P. Yadav and K. K. Saxena, *Mater. Today Proc.*, **18**, No. 2: 245 (2022); https://doi.org/10.1016/j.jmrt.2022.02.106
51. V.V. Girzhon, O.V.Smolyakov, O.V. Ovchinnikov, and O.V. Zavgorodny, *Metallofiz. Noveishie Tekhnol.*, **44**, No. 3: 383 (2022); https://doi.org/10.15407/mfint.44.03.0383
52. H.A. Wriedt and J.L. Murray, *Bull. Alloy Phase Diagrams*, **8**, No. 4: 378 (1987); https://doi.org/10.1007/BF02869274
53. V.V. Girzhon, O.V. Smolyakov, and T.A. Dmitrenko, *Metallofiz. Noveishie Tekhnol.*, **39**, No. 8: 1087 (2017) (in Russian);

https://doi.org/10.15407/mfint.39.08.1087
54. U. Mahajan, M. Dhonde, K. Sahu, P. Ghoshc, and P.M. Shirage, *Mater. Adv.*, **5**, 846 (2024);
https://doi.org/10.1039/D3MA00965C
55. Z. Wang, Y. Tan, and N. Li, J. Alloys Compd., **965**: 171030 (2023);
https://doi.org/10.1016/j.jallcom.2023.171030
56. A. Salihua, Y.I. Suleimanb, and A. I. Eyinavia, *AJER*, **8**, No. 8: 92 (2019).
57. Z.Z. Fang, J.D. Paramore, P. Sun, K.S. Ravi Chandran, Y. Zhang, Y. Xia, F. Cao, M. Koopman, and M. Free, *Int. Mater. Rev.*, **63**, No. 7: 407 (2018);
https://doi.org/10.1080/09506608.2017.1366003
58. Titanium Powder Metallurgy: Science, Technology and Applications (Eds. M. Qian and F.H. Froes) (Butterworth-Heinemann: 2015), p. 628;
https://doi.org/10.1016/C2013-0-13619-7
59. F.H. Froes, S.J. Mashl, J.C. Hebeisen, V.S. Moxson, and V.A. Duz, *JOM*, **56**: 46 (2004);
https://doi.org/10.1007/s11837-004-0252-x
60. I.V. Gaivoronskii, V.V. Girzhon, A.A. Skrebtsov, and A.V. Ovchinnikov, *Met. Sci. Heat Treat.*, **56**, Nos. 1–2: 57 (2014);
https://doi.org/10.1007/s11041-014-9703-3
61. G.A. Salishchev, R.M. Galeev, S.P. Malysheva, S.V. Zherebtsov, S.Yu. Mironov, O.R. Valiakhmetov, and É.I. Ivanisenko, *Met. Sci. Heat Treat.*, **48**, Nos. 1–2: 63 (2006);
https://doi.org/10.1007/s11041-006-0045-7
62. V.E. Olshanetskii, L.P. Stepanova, V.L. Greshta, D.V. Pavlenko, and D.V. Tkach, *Met. Sci. Heat Treat.*, **55**, Nos. 11–12: 603 (2014);
https://doi.org/10.1007/s11041-014-9676-2
63. R.A. Gaisin, V.M. Imayev, and R.M. Imayev, *Lett Mater.*, **7**, No. 2: 186 (2017);
https://doi.org/10.22226/2410-3535-2017-2-186-192
64. V.V. Girzhon and A.V. Ovchinnikov, *Met. Sci. Heat Treat.*, **58**, Nos. 11–12: 719 (2017);
https://doi.org/10.1007/s11041-017-0084-2
65. Y. Beygelzimer, *Mechan. Mater.*, **37**, No. 7: 735 (2005);
https://doi.org/10.1016/j.mechmat.2004.07.006
66. R.Z. Valiev, A.V. Sergueeva, and A.K. Mukherjee, *Scr. Mater.*, **49**, No. 7: 669 (2003);
https://doi.org/10.1016/S1359-6462(03)00395-6
67. V.V. Girzhon and I.V. Tahtsiura, *Metallofiz. Noveishie Tekhnol.*, **27**, No. 11: 1519 (2005).
68. I.P. Volchok, V.V. Girzhon, and I.V. Tantsiura, *Metallofiz. Noveishie Tekhnol.*, **33**, No. 8: 1111 (2011).
69. M.Kh. Abbas and A.K. Mahmoud, *Mater. Today Proc.*, **4**, No. 9: 9992 (2017);
https://doi.org/10.1016/j.matpr.2017.06.308
70. C. Dong, Z.K. Hei, L.B. Wang, Q.H. Song, Y.K. Wu, and K.H. Kuo, *Scr. Metal.*, **20**, No. 8: 1155 (1986);
https://doi.org/10.1016/0036-9748(86)90194-8
71. V.V. Girzhon, O.V. Smolyakov, and O.F. Zdorovets, *Metallofiz. Noveishie Tekhnol.*, **39**, No. 4: 507 (2017);
https://doi.org/10.15407/mfint.39.04.0507
72. H. Okamoto, M.E. Schlesinger, and E.M. Mueller, *Alloy Phase Diagrams* (ASM International: 2016), p. 1741;
https://doi.org/10.31399/asm.hb.v03.9781627081634
73. M. Bignon, E. Bertrand, P.E.J. Rivera-Díaz-del-Castillo, and F. Tancret, *J. Alloys Compd.*, **872**: 159636 (2021);
https://doi.org/10.1016/j.jallcom.2021.159636

Received 22.04.2024
Final version 02.11.2024

В.В. Гіржон[1], *О.В. Смоляков*[1], *В.Л. Грешта*[1],
В.В. Ємельянченко[1], *А.Ш. Раззоков*[2]
[1] Національний університет «Запорізька політехніка»,
вул. Жуковського, 64, 69063 Запоріжжя, Україна
[2] Ургенчський державний університет,
вул. Х. Алімджана, 14, 220100 Ургенч, Узбекистан

ЛАЗЕРНЕ ОБРОБЛЕННЯ ТИТАНОВИХ СПЛАВІВ

Методами рентгенівського та металографічного аналізу досліджено структурний і фазовий стани поверхневих шарів титанових сплавів ВТ1-0, ВТ3-1, ВТ-6 і ВТ-8 після лазерних оброблень у різних газових середовищах, сплаву ВТ25-У після гвинтової екструзії та подальшого лазерного оброблення, сплаву ВТ1-0 після лазерного легування порошками чистих елементів Fe, Co, Ni. Показано, що зазначені типи оброблень сприяють зростанню значень мікротвердості поверхневих шарів. Проаналізовано вплив атмосфери навколишнього газу та хімічного складу титанових сплавів на процеси структуроутворення і на значення мікротвердості оброблених шарів. Досліджено вплив лазерного оброблення поверхні спечених однофазних порошкових титанових сплавів типу ВТ1-0 на рівень пористості в зоні оплавлення. Встановлено, що мікротвердість у зоні лазерного оплавлення сплаву ВТ25У перевищує мікротвердість зразків після термічних оброблень і гвинтової екструзії. Тому наведені способи лазерного оброблення поверхонь є ефективним методом оброблення поверхні титанових сплавів, оскільки якісно впливають на структуру, що в свою чергу сприяє поліпшенню механічних характеристик поверхневих шарів.

Ключові слова: лазерне оброблення, лазерне легування, зона оплавлення, мартенситне перетворення, мікротвердість, фазовий склад.